Supporting Information

Endogenous Conjugation of Biomimetic Dinitrosyl Iron Complex with Protein Vehicles for Oral Delivery of Nitric Oxide to Brain and Activation of Hippocampal Neurogenesis

*Cheng-Ru Wu,[1,#] Yi-Da Huang,[1,2,#] Yong-Huei Hong,[1] Ya-Hsin Liu,[1] Manmath Narwane,[1] Yu-Hsiang Chang,[1] Trinh Kieu Dinh,[1] Hsin-Tzu Hsieh,[1] Yi-Jen Hseuh,[2] Ping-Ching Wu,[3] Chih-Wen Pao,[4] Ting-Shan Chan,[4] I-Jui Hsu,[5] Yunching Chen,[1] Hung-Chi Chen,[*2,6], Ting-Yu Ching,[*7], Tsai-Te Lu[*1]*

Affiliations:

[1]Institute of Biomedical Engineering, National Tsing Hua University, Hsinchu, Taiwan.

[2]Department of Ophthalmology and Center for Tissue Engineering, Chang Gung Memorial Hospital, Taoyuan, Taiwan

[3]Department of Biomedical Engineering, National Cheng Kung University, Tainan, Taiwan

[4]National Synchrotron Radiation Research Center, Hsinchu, Taiwan

[5]Department of Molecular Science and Engineering, Research and Development Center of Smart Textile Technology, National Taipei University of Technology, Taipei, Taiwan

[6]Department of Medicine, College of Medicine, Chang Gung University, Taoyuan, Taiwan

[7]Department of Bioscience Technology, Chung Yuan Christian University, Taoyuan, Taiwan

[#]C.-R.W. and Y.-D.H contributed equally.

[*]**Corresponding authors:**

Tsai-Te Lu, Ph.D., Institute of Biomedical Engineering, National Tsing Hua University, Hsinchu, Taiwan. E-mail: ttlu@mx.nthu.edu.tw.

Ting-Yu Chin, Ph.D., Department of Bioscience Technology, Chung Yuan Christian University, Taoyuan, Taiwan. E-mail: tychin@cycu.edu.tw.

Hung-Chi Chen, M.D. Ph.D., Department of Ophthalmology and Center for Tissue Engineering, Chang Gung Memorial Hospital, Linkou, Taiwan. E-mail: mr3756@cgmh.org.tw.

Scheme S1. Mechanism for degradation of **DNIC-1** (**a**) at pH 6.8 and (**b**) in SGFsp, respectively, under aerobic condition.

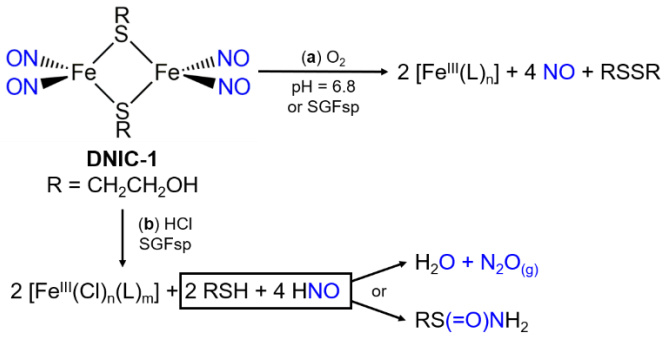

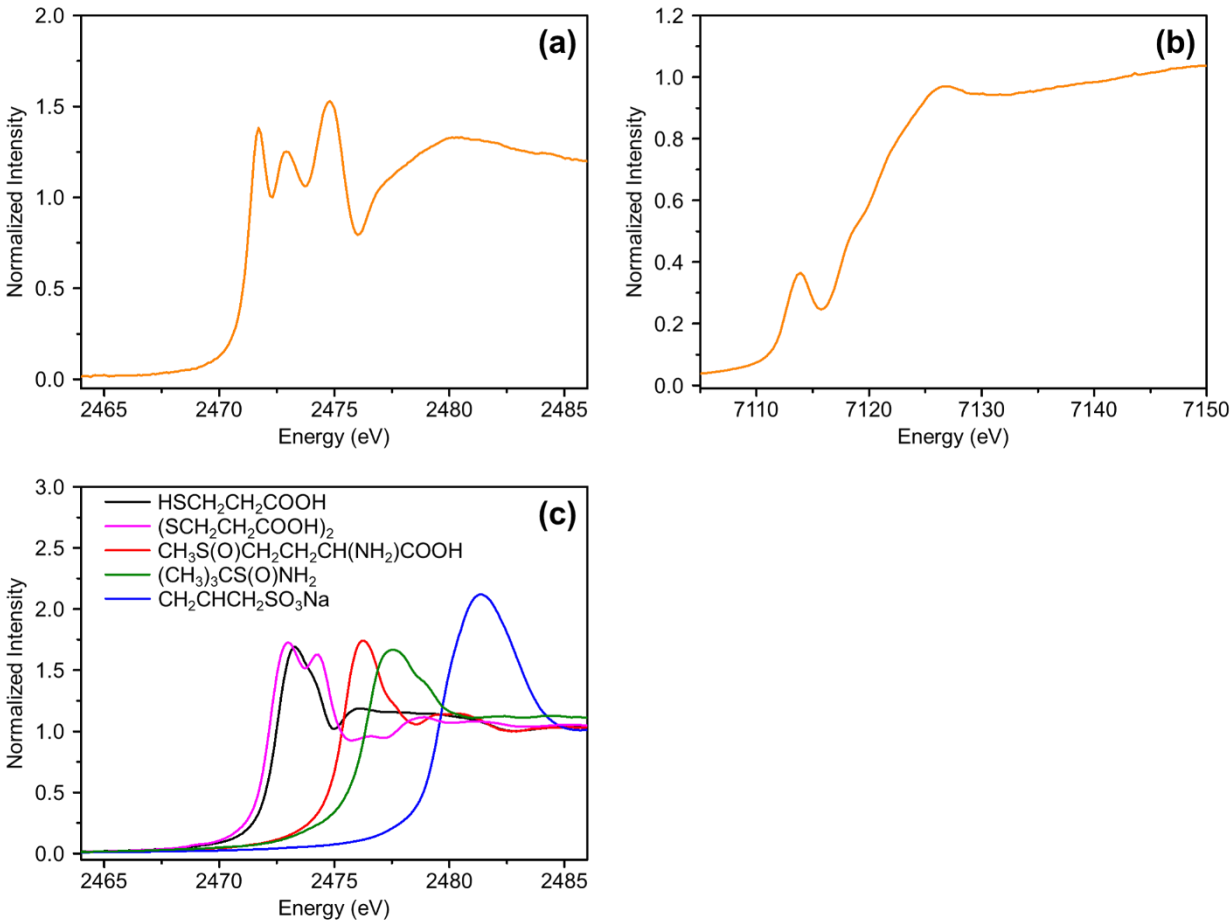

Figure S1. (**a**) S and (**b**) Fe K-edge X-ray absorption spectra for **DNIC-1**. (**c**) S K-edge X-ray absorption spectra for the $HSCH_2CH_2COOH$ (black), $(SCH_2CH_2COOH)_2$ (magenta), $CH_3S(O)CH_2CH_2CH(NH_2)COOH$ (red), $(CH_3)_3CS(O)NH_2$ (olive), and $CH_2CHCH_2SO_3Na$ (blue).

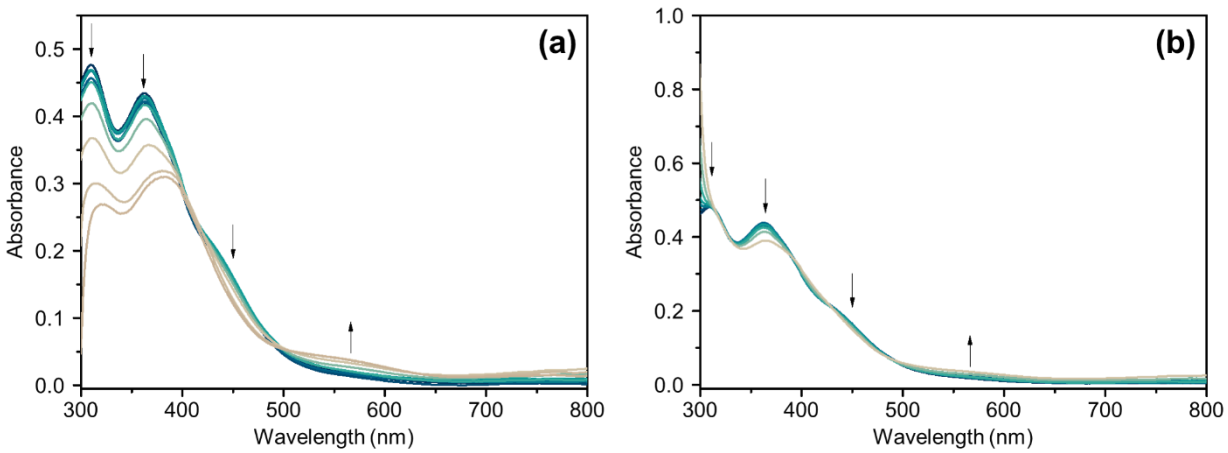

Figure S2. (**a**) UV-vis spectra for 50 μM of **DNIC-1** after addition of 0.25, 0.5, 0.75, 1.0, 1.25, 2.5, 5, 10, 25, and 50 mg/mL of bovine serum albumin (BSA) in PBS (pH 7.4). Change of UV-vis spectra during the titration was indicated by the arrow. Each UV-vis spectrum for this titration experiment was subtracted with the UV-vis spectrum of BSA at the corresponding concentration. (**b**) UV-vis spectra for 50 μM of **DNIC-1** after addition of 0.25, 0.5, 0.75, 1.0, 1.25, 2.5, 5, 10, 25, and 50 mg/mL of bovine serum albumin (BSA) in PBS (pH 7.4).

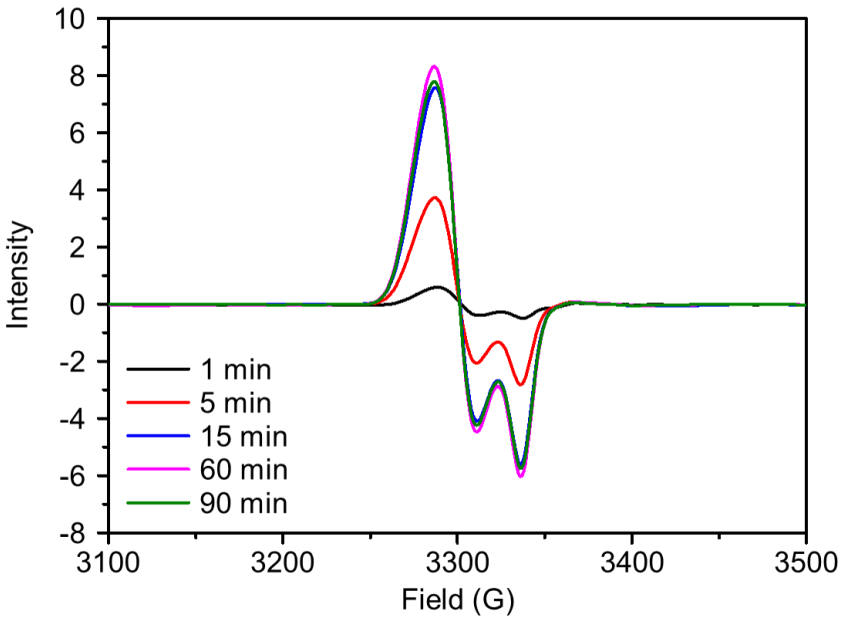

Figure S3. Reaction of **DNIC-1** and BSA monitored by EPR, which is performed under anaerobic condition.

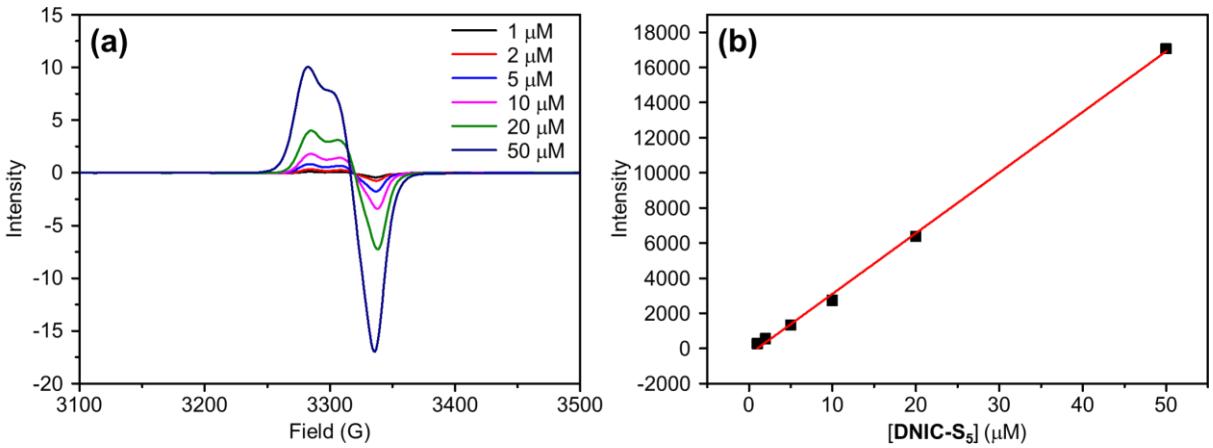

Figure S4. (**a**) EPR spectra for different concentration of [PPN][$(NO)_2Fe(S_5)$] (**DNIC-S_5**) in THF. (**b**) Calibration curve for **DNIC-S_5** in THF.

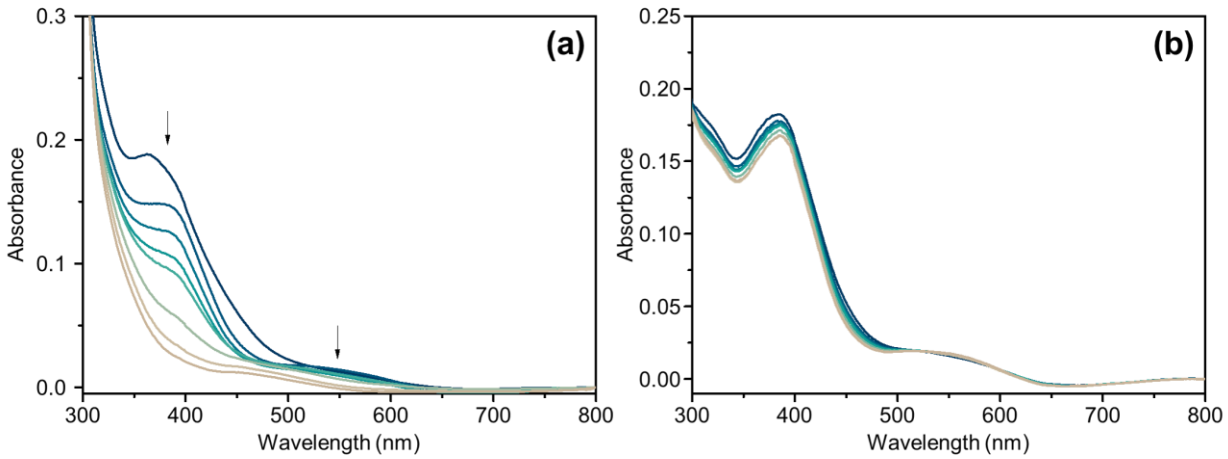

Figure S5. (**a**) Time-dependent change of UV-vis spectra for **DNIC-1** in the presence of BSA in PBS (pH 7.4) under aerobic condition at 37ºC. (**b**) Time-dependent change of UV-vis spectra for **DNIC-1** in the presence of BSA in PBS (pH 7.4) during its incubation under anaerobic condition at 37ºC for 24 h.

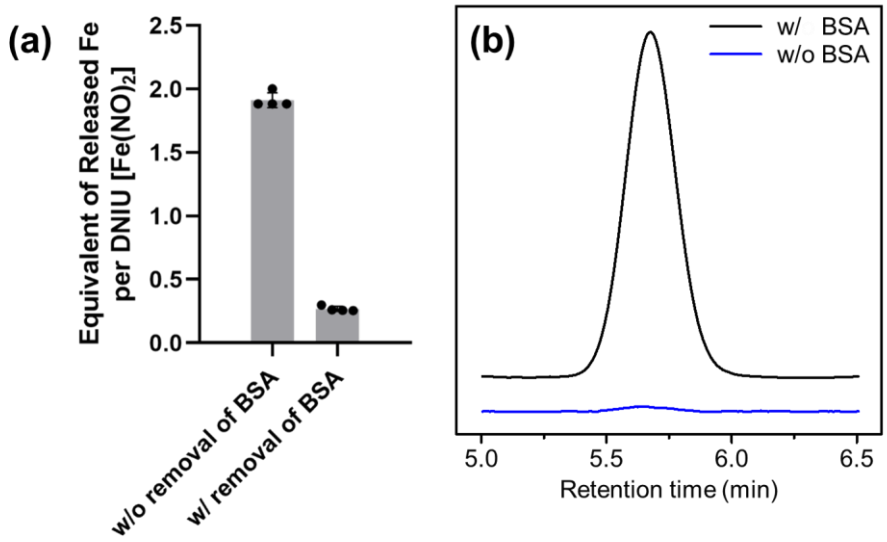

Figure S6. (**a**) Equivalent of released Fe per DNIU [$Fe(NO)_2$] after degradation of **DNIC-1** in the presence of BSA. ICP analysis on the supernatant solution was performed with or without removal of BSA adduct(s) by spin column. After removal of BSA adducts(s), significant decrease of equivalent of released Fe indicates the formation of BSA-bound Fe after degradation of **DNIC-1** in the presence of BSA. (**b**) GC chromatograms for the gaseous byproduct derived from decomposition of **DNIC-1** with (black) or without (blue) the presence of BSA in PBS (pH = 7.4).

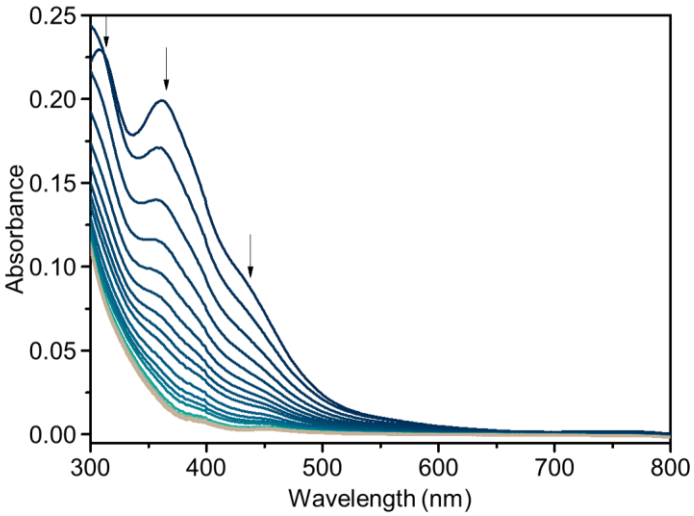

Figure S7. Time-dependent change of UV-vis spectra for 25 μM of **DNIC-1** in the presence of 150 μM of L-cysteine in PBS (pH 7.4) at 37^{o}C under aerobic condition.

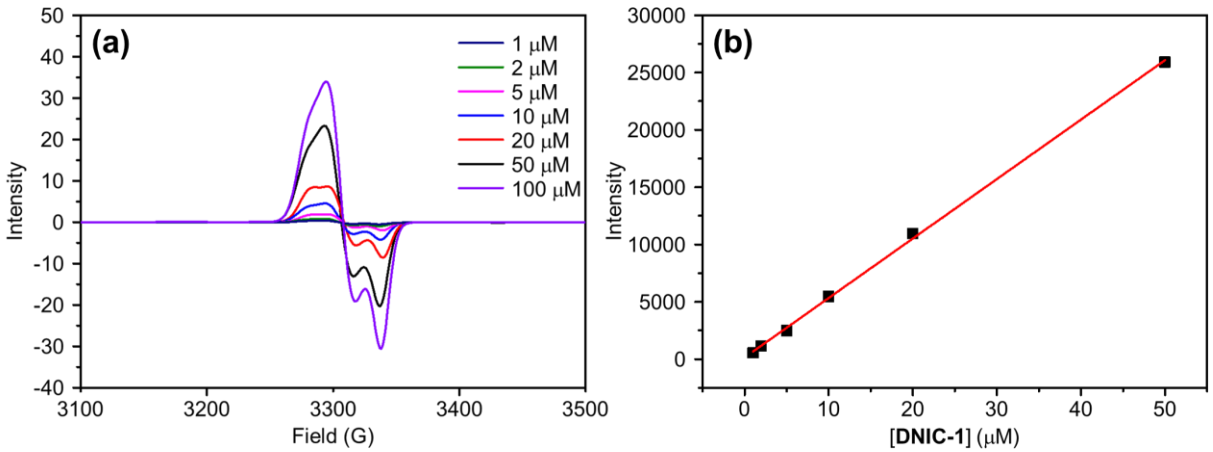

Figure S8. (**a**) EPR spectra for the isolated plasma after treatment with different concentration of **DNIC-1**. (**b**) Calibration curve for **DNIC-1** in the isolated plasma.

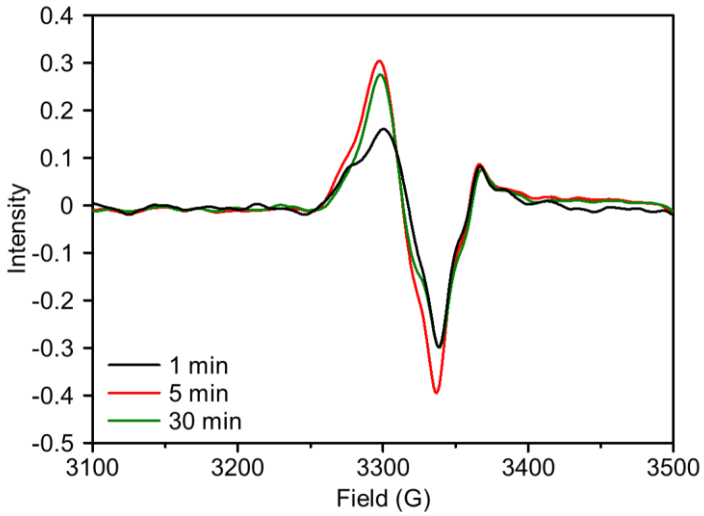

Figure S9. Reaction of **DNIC-1** and porcine stomach mucin in 100 mM phosphate buffer (pH 7.4) monitored by EPR, which is performed under aerobic condition.

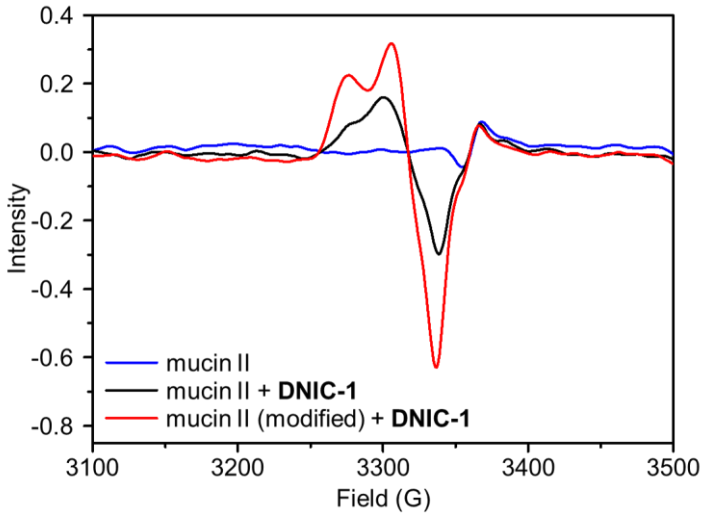

Figure S10. EPR spectra for reaction of **DNIC-1** with native (black) and NEM-modified mucin (red), respectively, in 100 mM phosphate buffer (pH 7.4). EPR spectrum of native mucin is shown in blue. Although the treatment of NEM fails to inhibit the formation of EPR-active and mucin-bound DNIC, the distinctive EPR spectra derived from reaction of **DNIC-1** with native and NEM-modified mucin, respectively, demonstrates the critical role of cysteine residue(s) for the formation of mucin-bound DNIC.

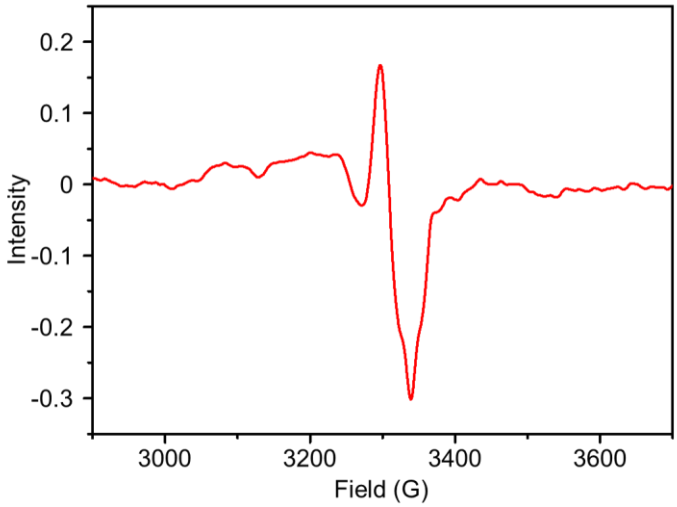

Figure S11. EPR spectrum for the stomach isolated from the mice with the oral administration of **DNIC-1**. This EPR spectrum for the stomach was collected after perfusion and removal of mucus.

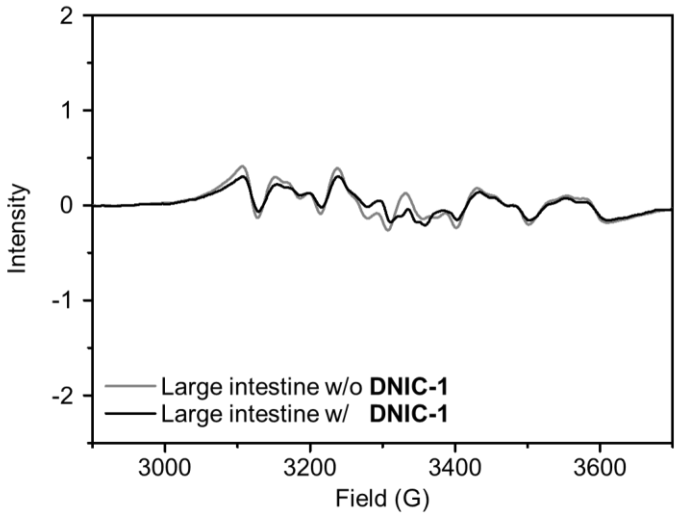

Figure S12. EPR spectra of large intestine isolated from the mice with (black) or without (gray) the oral administration of **DNIC-1**.

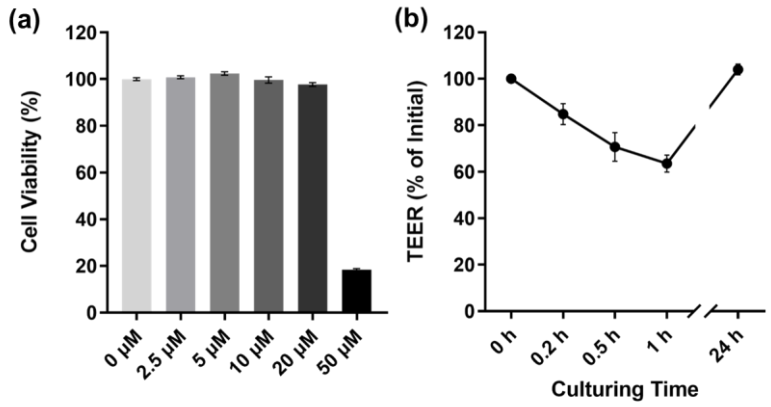

Figure S13. (**a**) Cell viability assay of the Caco-2 human intestinal epithelial cell treated with different concentration of **DNIC-1** for 24 h. (**b**) Effect of **DNIC-1** on time-dependent reduction of TEER in Caco-2 cell monolayer.

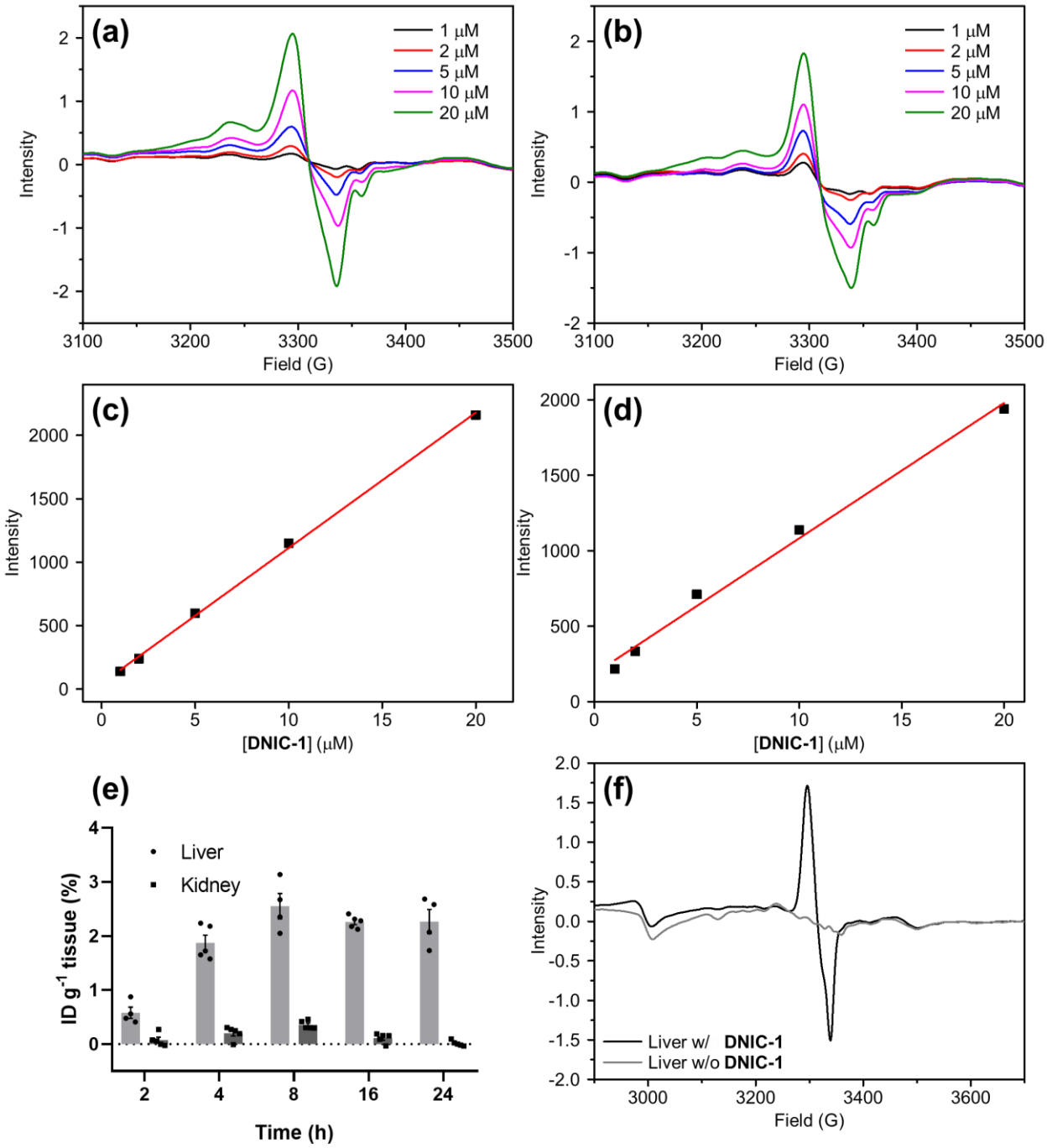

Figure S14. EPR spectra for different concentration of **DNIC-1** in the lysates of (**a**) liver and (**b**) kidney. Calibration curve for **DNIC-1** in the lysates of (**c**) liver and (**d**) kidney. (**e**) Time-dependent biodistribution study of **DNIC-1** in the liver (light gray) and kidney (dark gray). Data represent the mean ± SEM (n=4-5). ID g^{-1} tissue, injected dose per gram of tissue. (**f**) EPR spectra of liver isolated from the mice with (black) or without (gray) the oral administration of **DNIC-1**. Based on the EPR signal at g = 2.040, 2.028, 2.014, formation of protein-bound DNIC in the liver is relevant to the biomimetic DNICs $[(NO)_2Fe(SR)(L)]^-$ (Table S1, L = thiolate, amid, imidazolate, carboxylate, or phenoxide).

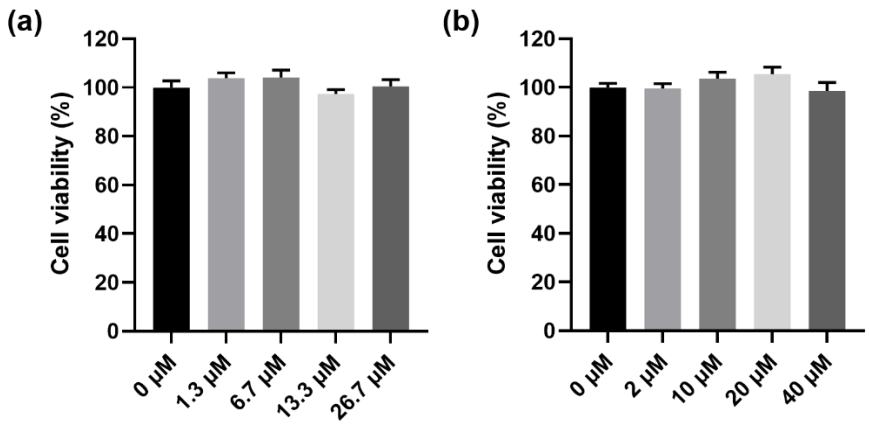

Figure S15. Cell viability assay of the N2A cells treated with different concentration of (**a**) 2-(*N*,*N*-diethylamino)-diazenolate 2-oxide (DEA NONOate) and (**b**) sodium nitroprusside (SNP), respectively, for 24. In this figure, the concentration of released nitric oxide from DEA NONOate (or SNP) is relevant to that from **DNIC-1** shown in Figure 4b.

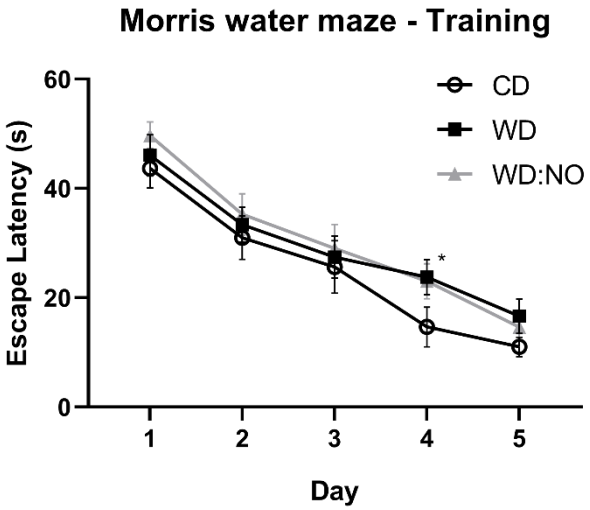

Figure S16. The time spent to reach the hidden platform (escape latency) during the acquisition phase of training (days 1-5 during week 17) in the Morris water maze task. $^{*}P < 0.05$ compared with the CD.

Table S1. EPR Parameters for Biomimetic, Peptide-bound, and Protein-bound $\{Fe(NO)_2\}^9$ DNICs.[a]

Biomimetic $\{Fe(NO)_2\}^9$ DNICs Featuring Tetrahedral Geometry[b]			
DNIC	Ligation Mode	EPR Parameters[c] (g_1, g_2, g_3)	Reference
$[(NO)_2Fe(S(CH_2)_3S)]^-$	(S,S)	(2.048, 2.033, 2.015)	1
$[(NO)_2Fe(S_5)]^-$	(S,S)	(2.049, 2.027, 2.015)	2
$[(NO)_2Fe(SEt)_2]^-$	(S,S)	(2.042, 2.027, 2.014)	3
$[(NO)_2Fe(S^tBu)_2]^-$	(S,S)	(2.039, 2.027, 2.013)	4
$[(NO)_2Fe(SC_6H_4$-*o*-$NCOPh)]^-$	(S,N)	(2.052, 2.033, 2.011)	5
$[(NO)_2Fe(SEt)(Im)]^-$	(S,N)	(2.037, 2.028, 2.014)	6
$[(NO)_2Fe(S^tBu)(Im)]^-$	(S,N)	(2.037, 2.027, 2.014)	6
$[(NO)_2Fe(SC_6H_4$-*o*-$COO)]^-$	(S,O)	(2.054, 2.036, 2.012)	5
$[(NO)_2Fe(SC_4H_3S)(OPh)]^-$	(S,O)	(2.038, 2.027, 2.013)	7
$[(NO)_2Fe(Im)_2]^-$	(N,N)	(2.040, 2.022, 2.013)	6
$[(NO)_2Fe(N_3)_2]^-$	(N,N)	(2.043, 2.023, 2.012)	5
$[(NO)_2Fe(C_{12}H_8N)_2]^-$	(N,N)	(2.029, 2.018, 2.011)	8
$[(NO)_2Fe(N(Mes)(TMS))_2]^-$	(N,N)	(2.022, 2.013, 2.005)	9
$[(NO)_2Fe(OPh)(Im)]^-$	(O,N)	(2.046, 2.021, 2.013)	7
$[(NO)_2Fe(OPh)_2]^-$	(O,O)	(2.041, 2.022, 2.013)	7
$[(NO)_2Fe(OPh\text{-}F)_2]^-$	(O,O)	(2.041, 2.024, 2.013)	7
Peptide-/Protein-bound $\{Fe(NO)_2\}^9$ DNICs			
Peptide/Protein	Ligation Mode	EPR Parameters	Ref.
L-cysteine	(S,S)	(2.04, 2.01)[f]	10
Glutathione	(S,S)	(2.04, 2.01)[f]	11
KCACK	(S,S)[d]	(2.040, 2.032, 2.014)	12
$KC(A)_2CK$	(S,S)[d]	(2.039, 2.029, 2.014)	12
$KC(A)_3CK$	(S,S)[d]	(2.040, 2.030, 2.014)	12
$KC(A)_4CK$	(S,S)[d]	(2.040, 2.029, 2.014)	12
Aconitase	(S,S)	(2.037, 2.031, 2.012)	13
SoxR	(S,S)[d]	(2.03, 2.012)[f]	14
FNR	(S,S)	(2.038, 2.034, 2.016)	15
Rieske-type [2Fe-2S] cluster	(S,S)	(2.032, 2.014)[f]	16
Endonuclease III	(S,S)	(2.042, 2.036, 2.015)	17
Hybrid cluster protein	(S,S)	(2.042, 2.028, 2.014)	18
Bovine serum albumin	(S,S)	(2.044, 2.034, 2.014)	This work
	(S,N)	(2.05, 2.04, 2.01)	10
	(N,N)	(2.055, 2.035, 2.01)	10
Porcine stomach mucin	(S,S)	(2.038, 2.028, 2.014)	This work
	(S,N)/(S,O)	(2.052, 2.026, 2.015)	This work
Mammalian ferritin	(S, S)	(2.033, 2.014)[f]	19
	(N,N)	(2.055, 2.033, 2.015)	19
Mammalian ferrochelatase	(S, S)	(2.033, 2.014)[f]	20
Human glutathione transferase (P1-1)	(S,O)[e]	(2.038, 2.028, 2.015)	21

[a]The EPR parameter for DNIC $[(NO)_2Fe(S_5)]^-$ was recorded at 4.2 K, whereas the EPR parameters for all the other DNICs collected in this Table were recorded at 77 K. [b]Five-coordinate and six-coordinate $\{Fe(NO)_2\}^9$ DNICs featuring EPR signal at g_{av} = 2.012-2.018 are not included in this Table.[22] [c]Biomimetic DNICs $[(NO)_2Fe(SR)(L)]^-$ (L = thiolate, amido, imidazolate, carboxylate, or phenoxide) feature a g_2 value of 2.036-2.027, whereas biomimetic DNICs $[(NO)_2Fe(L)_2]^-$ (L = imidazolate, azide, carbazolate, amide, and phenoxide) exhibit a smaller g_2 value of 2.024-2.013. [d]The ligation mode is verified by EXAFS. [e]The ligation mode is verified by single-crystal X-ray diffraction. [f]Axial EPR signal.

Table S2. Pharmacokinetic parameters for oral administration of DNIC-1 in C57BL/6JNarl mice.

	$t_{½}$ (h)	CL (L/h)	VD (L)	Bioavailability
DNIC-1	0.94±0.19	0.29	0.32	6.5%

Table S3. Body Weight and Biochemical Parameters of Aging Mice under Control Diet (CD), Western Diet (WD), and Western Diet in Combination with Daily Treatment of DNIC-1 (WD:NO) for 16 Weeks.[a]

Group	CD	WD	WD:NO
Body Weight (g)	32.26±4.11	43.37±8.45***	40.51±6.32***
Plasma glucose (mg/dL)	132.00±41.17	223.92±47.34***	152.75±45.75$^{\#\#}$
Serum TG (mg/dL)[b]	72.33±26.17	101.00±41.38	73.03±13.47
Serum TC (mg/dL)[b]	101.95±40.48	189.46±55.10***	165.95±39.80**
CRE (mg/dL)[b]	0.36±0.05	0.26±0.05*	0.32±0.04
UA (mg/dL)[b]	2.38±0.27	2.70±0.25	3.62±0.38
GOT (U/dL)[b]	73.20±66.19	133.80±98.25	76.00±57.65
GPT (U/dL)[b]	30.80±14.57	36.20±9.55	33.60±10.36$^{***, \#\#}$

[a]Each value represents the mean±SD (n = 11-12 for body weight in each group; n = 7-12 for plasma glucose, serum TG, and serum TC in each group; n = 5 for CRE, UA, GOT, and GPT in each group). $^{*}P < 0.05$, $^{**}P < 0.01$, and $^{***}P < 0.001$ compared with the CD; $^{\#\#}P < 0.01$ compared with the WD.
[b]TG = triacylglycerol, TC = total cholesterol, CRE = creatinine, UA = uric acid, GOT = glutamate oxaloacetate transaminase, GPT = glutamate pyruvate transaminase

References

1. Hung, M.-C.; Tsai, M.-C.; Lee, G.-H.; Liaw, W.-F., Transformation and structural discrimination between the neutral $\{Fe(NO)_2\}^{10}$ dinitrosyliron complexes (DNICs) and the anionic/cationic $\{Fe(NO)_2\}^9$ DNICs. *Inorg. Chem.* **2006,** *45* (15), 6041-6047.
2. Tsai, M.-L.; Chen, C.-C.; Hsu, I.-J.; Ke, S.-C.; Hsieh, C.-H.; Chiang, K.-A.; Lee, G.-H.; Wang, -. Y.; Chen, J.-M.; Lee, J.-F.; Liaw, W.-F., Photochemistry of the dinitrosyl iron complex $[S_5Fe(NO)_2]^-$ leading to reversible formation of $[S_5Fe(\mu\text{-}S)_2FeS_5]^{2-}$: spectroscopic characterization of species relevant to the nitric oxide modification and repair of [2Fe-2S] ferredoxins. *Inorg. Chem.* **2004,** *43* (16), 5159-5167.
3. Lu, T.-T.; Chiou, S.-J.; Chen, C.-Y.; Liaw, W.-F., Mononitrosyl tris(thiolate) iron complex $[Fe(NO)(SPh)_3]^-$ and dinitrosyl iron complex $[(EtS)_2Fe(NO)_2]^-$: formation pathway of dinitrosyl iron complexes (DNICs) from nitrosylation of biomimetic rubredoxin $[Fe(SR)_4]^{2-/1-}$ (R = Ph, Et). *Inorg. Chem.* **2006,** *45* (21), 8799-8806.
4. Tsou, C.-C.; Lu, T.-T.; Liaw, W.-F., EPR, UV-Vis, IR, and X-ray demonstration of the anionic dimeric dinitrosyl iron complex $[(NO)_2Fe(\mu\text{-}S^tBu)_2Fe(NO)_2]^-$: relevance to the products of nitrosylation of cytosolic and mitochondrial aconitases, and high-potential iron proteins. *J. Am. Chem. Soc.* **2007,** *129* (42), 12626-12627.
5. Tsai, M.-L.; Hsieh, C.-H.; Liaw, W.-F., Dinitrosyl iron complexes (DNICs) containing S/N/O ligation: transformation of Roussin's red ester into the neutral $\{Fe(NO)_2\}^{10}$ DNICs. *Inorg. Chem.* **2007,** *46* (12), 5110-5117.
6. Huang, H.-W.; Tsou, C.-C.; Kuo, T.-S.; Liaw, W.-F., New members of a class of dinitrosyliron complexes (DNICs): interconversion and spectroscopic discrimination of the anionic $\{Fe(NO)_2\}^9$ $[(NO)_2Fe(C_3H_3N_2)_2]^-$ and $[(NO)_2Fe(C_3H_3N_2)(SR)]^-$ ($C_3H_3N_2$ = deprotonated imidazole; R = ^{t}Bu, Et, Ph). *Inorg. Chem.* **2008,** *47* (6), 2196-2204.
7. Tsai, M.-C.; Tsai, F.-T.; Lu, T.-T.; Tsai, M.-L.; Wei, Y.-C.; Hsu, I.-J.; Lee, J.-F.; Liaw, W.-F., Relative Binding Affinity of Thiolate, Imidazolate, Phenoxide, and Nitrite Toward the $\{Fe(NO)_2\}$ Motif of Dinitrosyl Iron Complexes (DNICs): The Characteristic Pre-Edge Energy of $\{Fe(NO)_2\}^9$ DNICs. *Inorg. Chem.* **2009,** *48* (19), 9579-9591.
8. Lu, T.-T.; Chen, C.-H.; Liaw, W.-F., Formation of the distinct redox-interrelated forms of nitric oxide from reaction of dinitrosyl iron complexes (DNICs) and substitution ligands. *Chem. Eur. J.* **2010,** *16* (27), 8088-95.
9. Tsou, C.-C.; Tsai, F.-T.; Chen, H.-Y.; Hsu, I.-J.; Liaw, W.-F., Insight into One-Electron Oxidation of the $\{Fe(NO)_2\}^9$ Dinitrosyl Iron Complex (DNIC): Aminyl Radical Stabilized by $[Fe(NO)_2]$ Motif. *Inorg. Chem.* **2013,** *52* (3), 1631-1639.
10. Boese, M.; Mordvintcev, P. I.; Vanin, A. F.; Busse, R.; Mulsch, A., S-nitrosation of serum albumin by dinitrosyl-iron complex. *J. Biol. Chem.* **1995,** *270* (49), 29244-29249.
11. Lo Bello, M.; Nuccetelli, M.; Caccuri, A. M.; Stella, L.; Parker, M. W.; Rossjohn, J.; McKinstry, W. J.; Mozzi, A. F.; Federici, G.; Polizio, F.; Pedersen, J. Z.; Ricci, G., Human glutathione transferase P1-1 and nitric oxide carriers. *J. Biol. Chem.* **2001,** *276* (45), 42138-42145.
12. Lin, Z.-S.; Lo, F.-C.; Li, C.-H.; Chen, C.-H.; Huang, W.-N.; Hsu, I.-J.; Lee, J.-F.; Horng, J.-C.; Liaw, W.-F., Peptide-bound dinitrosyliron complexes (DNICs) and neutral/reduced-form Roussin's red esters (RREs/rRREs): understanding nitrosylation of [Fe-S] clusters leading to the formation of DNICs and RREs using a de novo design strategy. *Inorg. Chem.* **2011,** *50* (20), 10417-10431.
13. Kennedy, M. C.; Antholine, W. E.; Beinert, H., An EPR investigation of the products of the reaction of cytosolic and mitochondrial aconitases with nitric oxide. *J. Biol. Chem.* **1997,** *272* (33), 20340-20347.
14. Lo, F. C.; Lee, J. F.; Liaw, W. F.; Hsu, I. J.; Tsai, Y. F.; Chan, S. I.; Yu, S. S., The metal core structures in the recombinant *Escherichia coli* transcriptional factor SoxR. *Chem. Eur. J.* **2012,** *18* (9), 2565-2577.
15. Cruz-Ramos, H.; Crack, J.; Wu, G.; Hughes, M. N.; Scott, C.; Thomson, A. J.; Green, J.; Poole, R. K.,

NO sensing by FNR: regulation of the Escherichia coli NO-detoxifying flavohaemoglobin, Hmp. *EMBO J.* **2002,** *21* (13), 3235-3244.
16. Tinberg, C. E.; Tonzetich, Z. J.; Wang, H.; Do, L. H.; Yoda, Y.; Cramer, S. P.; Lippard, S. J., Characterization of iron dinitrosyl species formed in the reaction of nitric oxide with a biological Rieske center. *J. Am. Chem. Soc.* **2010,** *132* (51), 18168-18176.
17. Ekanger, L. A.; Oyala, P. H.; Moradian, A.; Sweredoski, M. J.; Barton, J. K., Nitric Oxide Modulates Endonuclease III Redox Activity by a 800 mV Negative Shift upon [Fe_4S_4] Cluster Nitrosylation. *J. Am. Chem. Soc.* **2018,** *140* (37), 11800-11810.
18. Hagen, W. R., EPR spectroscopy of putative enzyme intermediates in the NO reductase and the auto-nitrosylation reaction of Desulfovibrio vulgaris hybrid cluster protein. *FEBS Lett.* **2019,** *593* (21), 3075-3083.
19. Lee, M.; Arosio, P.; Cozzi, A.; Chasteen, N. D., Identification of the EPR-active iron-nitrosyl complexes in mammalian ferritins. *Biochemistry* **1994,** *33* (12), 3679-3687.
20. Sellers, V. M.; Johnson, M. K.; Dailey, H. A., Function of the [2Fe-2S] cluster in mammalian ferrochelatase: A possible role as a nitric oxide sensor. *Biochemistry* **1996,** *35* (8), 2699-2704.
21. Cesareo, E.; Parker, L. J.; Pedersen, J. Z.; Nuccetelli, M.; Mazzetti, A. P.; Pastore, A.; Federici, G.; Caccuri, A. M.; Ricci, G.; Adams, J. J.; Parker, M. W.; Lo Bello, M., Nitrosylation of human glutathione transferase P1-1 with dinitrosyl diglutathionyl iron complex in vitro and in vivo. *J. Biol. Chem.* **2005,** *280* (51), 42172-42180.
22. Tsai, M.-L.; Tsou, C.-C.; Liaw, W.-F., Dinitrosyl iron complexes (DNICs): from biomimetic synthesis and spectroscopic characterization toward unveiling the biological and catalytic roles of DNICs. *Acc. Chem. Res.* **2015,** *48* (4), 1184-1193.